

Observations of second-harmonic generation from randomly rough metal surfaces

K. A. O'Donnell

The School of Physics, Georgia Institute of Technology, Atlanta, Georgia 30332

R. Torre

European Laboratory for Nonlinear Spectroscopy, Largo Enrico Fermi 2, Florence 50125, Italy

C. S. West

The School of Physics, Georgia Institute of Technology, Atlanta, Georgia 30332

(Received 12 August 1996)

The angular distributions of second-harmonic light scattered from metal surfaces with weak random roughness are studied experimentally. The power spectrum of the roughness has a rectangular form centered on the surface plasmon polariton wave number at the fundamental frequency, producing strong excitation of these surface waves. The scattering distributions exhibit a pair of distinct peaks at angles consistent with the nonlinear interaction of the incident wave with fundamental plasmon polaritons. The controlled experiments allow a number of other scattering processes to be identified that include, for example, the nonlinear excitation of surface plasmon polaritons at the harmonic frequency. A peak in the second-harmonic distribution, predicted to appear in a direction perpendicular to the mean surface, is not observed. [S0163-1829(97)01911-5]

I. INTRODUCTION

Little past research has considered the nonlinear optical interactions occurring on a metal surface having random roughness. It is well known that even a flat metal surface may produce effects such as the generation of second-harmonic light in a specularly reflected laser beam.^{1,2} However, a surface with random roughness represents a considerably more complex situation that would be expected to produce diffuse scatter in the second harmonic. The form of the associated angular scattering distribution should be governed by the strength of the nonlinear interactions occurring between all waves present at the surface. This is indeed the case in lowest-order roughness perturbation theory,³ in which the second-harmonic distribution arises from the nonlinear coupling between the incident wave and the fundamental diffuse scatter of lowest order. Generally, a broad distribution was predicted having two distinct peaks due to the nonlinear interaction of the incident wave with surface plasmon polaritons. Studies of higher-order perturbation terms have also predicted, at much lower levels, narrow peaks in the backscattering direction and in a direction normal to the mean surface.³

We are unaware of any experimental observations that are qualitatively consistent with even the lowest-order theory, where the incident wave/polariton interaction peaks should be quite obvious. For a rough free-space/metal interface we are aware only of the work of Chen, de Castro, and Shen,⁴ who do not show angle-resolved results explicitly but describe a nearly isotropic distribution in the second harmonic. We attribute the shortage of reported experiments to the inherent weakness of the light distribution; obtaining observable second-harmonic signals even upon specular reflection from a flat metal may require incident power levels near those destroying the sample.^{1,2} This situation is quite different from analogous studies of metallic diffraction gratings,

where theoretical works⁵ have been balanced by experimental studies of second-harmonic light emitted into isolated diffracted orders,^{6,7} the detected signals were generally weak but adequate.

We thus present here an experimental study of the second-harmonic scattering distributions occurring for a free-space/silver interface having weak random roughness. The experiments to be described are unusual for several reasons. First, the surface roughness is fully characterized with a profilometer and all scattering data are absolutely normalized. Further, the power spectrum of the roughness has a rectangular form centered on the surface plasmon polariton wave number at the fundamental frequency, which produces extremely strong excitation of these surface waves. This spectrum is quite different from the common theoretical assumption of a broad Gaussian spectrum centered on zero wave number.³ It will be seen that our relatively narrow rectangular spectrum allows the dominant nonlinear coupling processes to be identified from the form of the second-harmonic scattering distributions, thus providing a clear and unambiguous interpretation of results.

Even though the nature of these distributions should be considered an open issue at this point, the surface wave excitation suggests that the two related peaks of the lowest-order second-harmonic scattering should be present. In Sec. II, after the fabrication and characterization of the rough surfaces are described, we further demonstrate that the linear diffuse scatter contains a backscattering enhancement peak.³ It has been discussed by McGurn, Leskova, and Agranovich³ (MLA) that this peak must exist to produce the second-harmonic peak in the direction perpendicular to the surface. Particular attention is thus given to this direction as we present the second-harmonic scattering distributions in Sec. III. In our discussion of the results in Sec. IV, we consider the contributions observed from yet other nonlinear scattering processes.

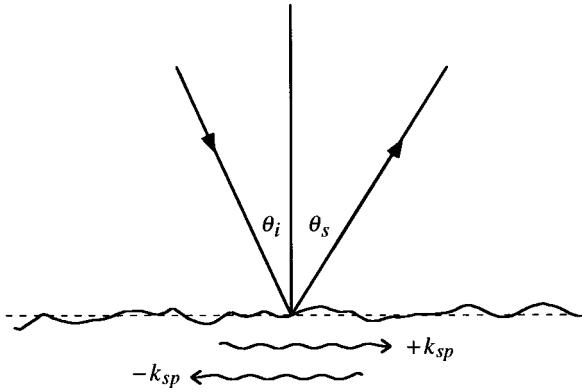


FIG. 1. Scattering of light by a rough metal surface. The angle of incidence θ_i and the angle of scattering θ_s are positive, as shown.

Over the past 30 years, much theoretical effort has been directed toward the development of models for the nonlinear polarization of metal surfaces.^{1,2,8} Such theories have generally been tested through comparison with experimental studies of specularly reflected second-harmonic generation. However, it will be seen here that random roughness allows a much wider variety of nonlinear wave interactions to occur simultaneously on a metal surface. Even though our discussion will be restricted to a qualitative interpretation of the nonlinear processes observed, our controlled experimental results may ultimately provide far more stringent tests of these important theoretical models.

II. EXPERIMENTAL TECHNIQUES

The surfaces described here have highly one-dimensional roughness, as is widely assumed in theoretical works. As shown in Fig. 1, the roughness is intended to couple a light wave incident at angle θ_i to counterpropagating surface plasmon polaritons at the fundamental frequency ω . This condition implies that there must be wave numbers k_r and k_r' present in the roughness's power spectrum $S(k)$ that satisfy the coupling equations

$$+k_{sp}(\omega) = k_i(\omega) + k_r, \quad -k_{sp}(\omega) = k_i(\omega) - k_r', \quad (1)$$

where $k_i(\omega) = (\omega/c)\sin\theta_i$ is the component of the incident wave vector parallel to the mean surface and $\pm k_{sp}(\omega)$ is the wave number of the polariton traveling to the right (+) or left (-) along the surface. For a limited range of θ_i (in particular, for $|\theta_i| \leq \theta_{\max}$, where θ_{\max} is a maximum coupling angle) it is straightforward to show that Eqs. (1) are satisfied as long as $S(k)$ is nonzero within a full width $\Delta k = (2\omega/c)\sin\theta_{\max}$ centered on $k_{sp}(\omega)$. For simplicity, our surfaces were thus fabricated so that $S(k)$ was significant only within this essential region. Assuming the final experiment would employ illumination wavelength 1064 nm, we determine that $S(k)$ should be centered at $k_{sp}(\omega) = \text{Re}[\sqrt{\epsilon/(\epsilon+1)}](\omega/c) = 1.0097(\omega/c)$ from the dielectric constant ϵ of silver.⁹ We determine Δk by choosing $\theta_{\max} = 15^\circ$.

The surfaces were made using extensions of holographic grating fabrication techniques.¹⁰ To prepare each surface, a $50 \times 50 \text{ mm}^2$ glass plate was coated with a $1.5\text{-}\mu\text{m}$ layer of

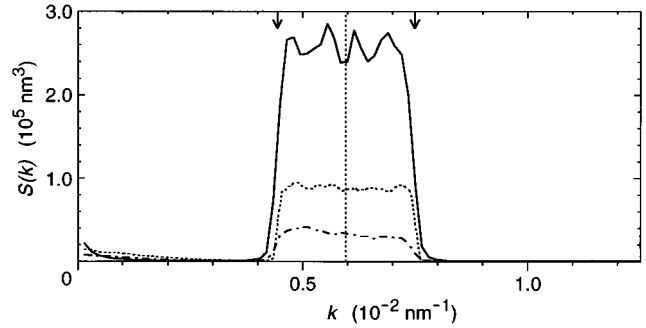


FIG. 2. Power spectrum $S(k)$ of the surface roughness as determined from profilometer data for surfaces 1 (dot-dashed curve), 2 (dashed curve), and 3 (solid curve). The dashed vertical line appears at $k_{sp}(\omega)$ and the arrows denote the desired spectral limits. Results are normalized such that the area equals the variance σ^2 of the surface roughness.

Shipley S1400-27 photoresist. The plate was exposed to a large number N of sinusoidal intensity distributions arising at the intersection of two light beams. The source was a HeCd laser of wavelength 442 nm. Each sinusoidal pattern had a different spatial wave number k in the direction along the plate and was randomly phased with respect to all other exposures. With the exposure wave numbers evenly spaced along the k axis within the bandwidth Δk , the net exposure behaves as a Fourier series that, in the limit of large N , becomes consistent with a Gaussian random process.¹⁰ The plate was then developed in a manner producing a linear relation between exposure and resulting surface height (30 sec in Shipley 352 developer).

After a thick layer (400 nm) of silver was evaporated onto the sample at a pressure less than 10^{-6} Torr, it was characterized with a Talystep stylus profilometer. The spectrum $S(k)$ was computed from the profilometer data and is shown in Fig. 2 for each of the three surfaces employed here. Surface 1 ($N=3000$, rms roughness $\sigma=10.8$ nm), surface 2 ($N=1200$, $\sigma=17.3$ nm), and surface 3 ($N=500$, $\sigma=28.3$ nm) all exhibit a similar rectangular spectral form. The measured spectra are centered on $k_{sp}(\omega)$ and are significantly nonzero only within the desired bandwidth Δk . While not in use, the samples were kept in an inert gas atmosphere.

As discussed in the Introduction, peaks both in the backscattering direction and in the direction normal to the mean surface were predicted by MLA. The former peak is due to the excitation of $\pm k_{sp}(2\omega)$, but the coupling mechanism requires roughness wave numbers in regions where $S(k)$ is negligible in Fig. 2. On the other hand, the peak normal to the surface depends on the excitation of $\pm k_{sp}(\omega)$, so that our surfaces appear to be well suited to observe only the latter effect. We can provide more direct evidence of this assertion. As described by MLA, the peak perpendicular to the surface arises from the nonlinear interaction between the incident wave and the scattered waves of a backscattering enhancement peak at frequency ω . We thus demonstrate here the existence of this peak in the linear diffuse scatter.

The backscattering enhancement arises from the roughness coupling of the surface plasmon polaritons to outgoing waves.^{11,12} The outward coupling may be described by equations analogous to Eq. (1) as

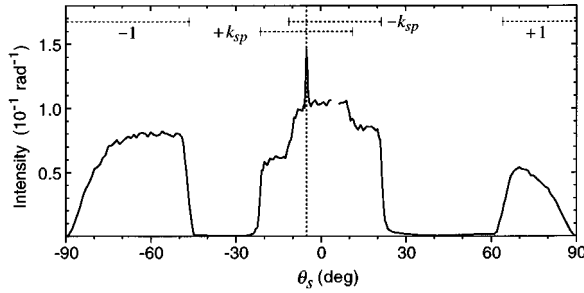


FIG. 3. Linear diffusely scattered intensity from surface 3 for p polarization, wavelength 1152 nm, and $\theta_i = 5^\circ$. The dashed vertical line denotes the direction of backscattering. Horizontal lines denote the outward coupling ranges of $\pm k_{sp}$ [Eqs. (2)] and of single scatter [± 1 , depending on the sign of Eq. (3)], evaluated at the actual frequency used. The detector integration angle $\Delta\theta_s = 0.4^\circ$.

$$k_s(\omega) = +k_{sp}(\omega) - k_r, \quad k_s(\omega) = -k_{sp}(\omega) + k_r', \quad (2)$$

where $k_s(\omega) = (\omega/c)\sin\theta_s$ is the component of the scattered wave vector parallel to the mean surface, k_r and k_r' are again suitable roughness wave numbers, and θ_s is the angle of scatter of Fig. 1. From Eqs. (2) it immediately follows that the outward coupling is confined to $|\theta_s| \leq \theta_{\max}$ for the rectangular spectrum. The peak should persist at backscattering ($\theta_s = -\theta_i$) as long as $|\theta_i| \leq \theta_{\max}$; outside this range both the inward and outward roughness couplings are forbidden.

We do not have a source of wavelength 1064 nm that is convenient to use in a linear scattering experiment, but instead employ a HeNe laser of wavelength 1152 nm and an instrument discussed elsewhere.¹⁰ The mean diffusely scattered intensity in p polarization is shown in Fig. 3 for surface 3 at $\theta_i = 5^\circ$, where a backscattering peak is clearly seen. The substantial amount of source detuning manifests itself as an angular shift between the distributions created by $+k_{sp}(\omega)$ and $-k_{sp}(\omega)$,¹³ as may be verified by evaluating Eqs. (2) at the actual frequency used in Fig. 3. The diffuse scatter for θ_s near grazing may be attributed to single scatter as in

$$k_s(\omega) = k_i(\omega) \pm k_r, \quad (3)$$

where k_r is again a roughness wave number available in $S(k)$. In particular, the edges of these distributions agree well with the angular limits obtained in Eq. (3) with k_r equal to the minimum wave number present in $S(k)$.

It will be seen that nonlinear mechanisms excite surface plasmon polaritons at frequency 2ω in the experiments of Sec. III, so that we consider here the consequences of their excitation. For example, if $+k_{sp}(2\omega)$ is excited, it may be roughness coupled to outgoing waves through a version of Eqs. (2) at 2ω as

$$k_s(2\omega) = +k_{sp}(2\omega) - k_r, \quad (4)$$

where $k_s(2\omega) = (2\omega/c)\sin\theta_s$, and we estimate from Ref. 9 that $k_{sp}(2\omega) = 1.052(2\omega/c)$. For our form of $S(k)$, Eq. (4) predicts that the outward coupling should be constrained to θ_s within $(25^\circ, 43^\circ)$. This outward diffuse coupling may be readily observed by launching $+k_{sp}(2\omega)$ through roughness coupling of an incident light wave of frequency 2ω . From inward coupling considerations [a version of Eqs. (1) at

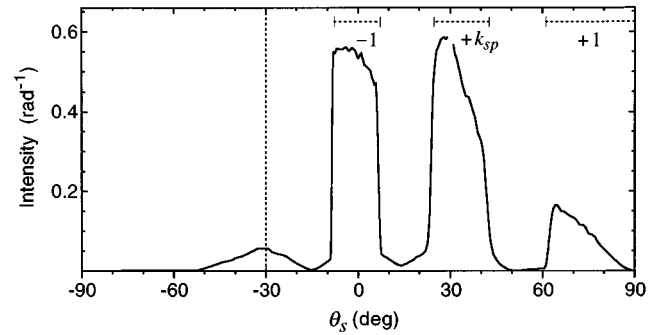


FIG. 4. Linear diffusely scattered intensity from surface 3 for p polarization, wavelength 543 nm, and $\theta_i = 30^\circ$. The dashed vertical line is the direction of backscattering. Horizontal lines denote the outward coupling ranges of $+k_{sp}(2\omega)$ [Eq. (4)] and of single scatter [from Eq. (3) at 2ω , where ± 1 denotes the sign in Eq. (3)]. The detector integration angle $\Delta\theta_s = 0.7^\circ$.

2ω] it is readily shown that $+k_{sp}(2\omega)$ should be excited in this manner for θ_i also within $(25^\circ, 43^\circ)$.

Again, we do not have a convenient light source of frequency 2ω and instead use a HeNe laser of wavelength 543 nm. The p -polarized diffuse intensity is shown in Fig. 4 for surface 3 with $\theta_i = 30^\circ$. A distribution clearly rises within the calculated angular limits, demonstrating the diffuse outward coupling of the right-traveling surface wave. Diffuse scatter also rises through single-scatter mechanisms [analogous to Eq. (3) at frequency 2ω] within the predicted angular limits, although these couplings are not of our direct interest. The source detuning is small and only the actual 2ω coupling ranges are shown for simplicity; they remain within 1° of those of the light source used here. Finally, although we do not present further data, scattering distributions similar to Figs. 3 and 4 have been observed for surfaces 1 and 2.

III. EXPERIMENTAL RESULTS

In the experiments studying second-harmonic generation, pulses from a mode-locked Coherent Antares Nd:YAG laser (where YAG denotes yttrium aluminum garnet) were sent to a Spectra Physics 3800RA regenerative amplifier. The output pulses thus obtained were of wavelength 1064 nm, full width at half maximum 100 psec, peak power 10 MW, and repetition rate 1 kHz. The slightly convergent incident beam was p polarized and had transverse e^{-1} intensity radius $w = 2.0$ mm at the sample. The scattering instrument was of geometry identical to that used in the linear experiments of Sec. II, with a detector arm mounted on a motorized rotation stage to produce scans in θ_s along the plane of incidence. The sample was mounted on a concentric rotation stage to set θ_i . In front of the detector, a slit 60 cm from the surface determined the detector integration angle $\Delta\theta_s$. The scattered light then passed through an infrared-absorbing Schott BG39 filter and an interference filter centered at 532 nm with a bandwidth of either 3 or 10 nm and was finally focused by a field lens onto a photon-counting photomultiplier. To remove speckle noise, the sample was translated over the uniformly rough surface area (27 mm width) as the detector signal was averaged to provide each data point.

A Stanford Research SR400 counter was gated to accept

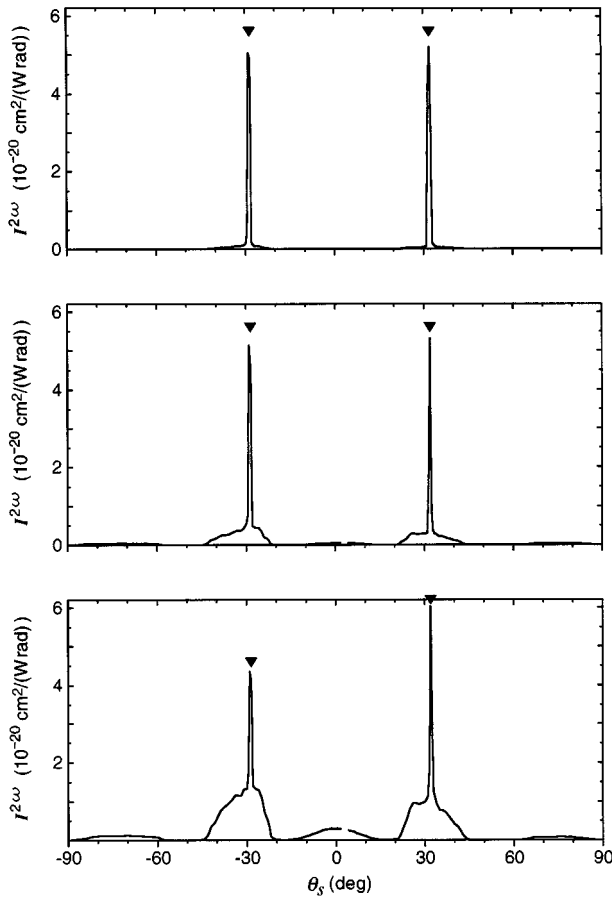


FIG. 5. Diffusely scattered second-harmonic $I^{2\omega}$ for surfaces 1 (top), 2 (center), and 3 (bottom). The illumination wavelength is 1064 nm, θ_i is 3° , and inverted triangles denote θ_s determined from $k_s(2\omega) = k_i(\omega) \pm k_{sp}(\omega)$. The detector integration angle $\Delta\theta_s = 0.8^\circ$. The break in each curve surrounds the specular reflection.

photoelectric counts within a 5-nsec window coincident with each laser pulse. The deadtime was 5 nsec, which implies that more than one count per laser pulse would be treated as a single count. Rates were thus kept low to avoid counter-saturation. The count rate was verified to be linearly proportional to detected second-harmonic power for rates up to 150 sec^{-1} and, when signals approached this level, the isolated second-harmonic light was attenuated with calibrated filters. In all figures, count rates that appear to exceed 150 sec^{-1} were actually at lower rates with an attenuation filter and were later corrected for this filter.

We have also made efforts to calibrate the scattering instrument and thus to provide absolute normalization of results. Our main results are expressed as a diffuse second-harmonic intensity $I^{2\omega}$ with units $\text{cm}^2/\text{W rad}$; this is analogous to the units cm^2/W commonly used for second-harmonic generation upon specular reflection.² To determine the scattering distribution in W/rad with the sample illuminated by a continuous source of power P , it is necessary to multiply $I^{2\omega}$ by P^2 and to divide by an effective transverse area $2\pi w^2$ of the illuminating beam.

Figure 5 shows the scattering distributions $I^{2\omega}$ for surfaces 1, 2, and 3 with $\theta_i = 3^\circ$. For the surface with weakest roughness, only two narrow peaks are apparent in $I^{2\omega}$. For

surface 2 these peaks appear with the same height, but are now surrounded by lower levels of diffuse scatter. In the case of surface 3, the peaks become somewhat asymmetric as the distributions surrounding them continue to rise. Further, surface 3 produces diffuse scatter for small θ_s as well as for θ_s near grazing. We may compare these results qualitatively with those of lowest-order perturbation theory,³ which predicts that the incident wave/polariton interaction peaks will occur for θ_s satisfying $k_s(2\omega) = k_i(\omega) \pm k_{sp}(\omega)$. It can be seen in Fig. 5 that the calculated angles agree with the observed peak positions, thus demonstrating the physical origin of the peaks.

However, it is remarkable that the peak heights are nearly constant throughout Fig. 5 and do not rise significantly as σ increases. In fact, in lowest-order perturbation theory³ the peak height is proportional to σ^2 and, for the surface parameters quoted earlier, the peaks for surface 3 would be 6.9 times higher than for surface 1. Thus, while the scattering mechanisms producing the experimental peaks are consistent with this theory, we must conclude that we are well outside the domain of validity of the prediction of this theory for the peak height. The lack of a significant increase in peak height indicates that perturbation theory has failed even for surface 1, although $\sigma/\lambda = 0.010$ remains a small perturbation parameter.

There are signals below levels that can be seen in Fig. 5, so these results are also presented with an expanded vertical scale in Fig. 6. For all three surfaces, there are ranges of θ_s where $I^{2\omega}$ is significant, with intermediate regions where coupling appears to be forbidden. All surfaces emit diffuse scatter near grazing for $\theta_s < -59^\circ$ and $\theta_s > 65^\circ$, while other distributions surround the incident wave/polariton interaction peaks. Further, surface 1 produces a nearly rectangular distribution within $(-5^\circ, 9^\circ)$ that occurs with a smoother form for surface 2, but this distribution appears with a nearly triangular form with a greater width for surface 3. It seems reasonable to attribute the series of allowed and forbidden outward coupling seen in $I^{2\omega}$ in Fig. 6 to the narrow bandwidth of $S(k)$, although we delay a discussion of this point until Sec. IV.

In Fig. 7 we present a study of $I^{2\omega}$ for surface 3 at three incidence angles. It can be seen that the incident wave/polariton interaction peaks are of equal height at $\theta_i = 0^\circ$, but the peak at positive θ_s becomes higher for $\theta_i = 8^\circ$ and 13° . The observed angular positions of the peaks agree well with the calculated angles throughout the results. These same results for $I^{2\omega}$ are also shown with an expanded vertical scale in Fig. 8. As θ_i increases, it is clear that the scatter for θ_s near grazing moves to the right, but the distributions surrounding the incident wave/polariton interaction peaks remain at nearly fixed angles.

The surface plasmon polariton excitation ceases when the roughness coupling breaks down for $\theta_i > 15^\circ$, as was discussed in Sec. II. Figure 8 shows the remarkable consequences on $I^{2\omega}$ in a case for $\theta_i = 17^\circ$. It is seen that the two narrow peaks disappear, as should be expected without polariton excitation. However, almost all other components of $I^{2\omega}$ have also disappeared and only some low levels of scatter remain for $41^\circ < \theta_s < 68^\circ$. What appear to be these same low scattering levels are seen to be emerging from the stronger scatter for $44^\circ < \theta_s < 59^\circ$ with $\theta_i = 13^\circ$ and for

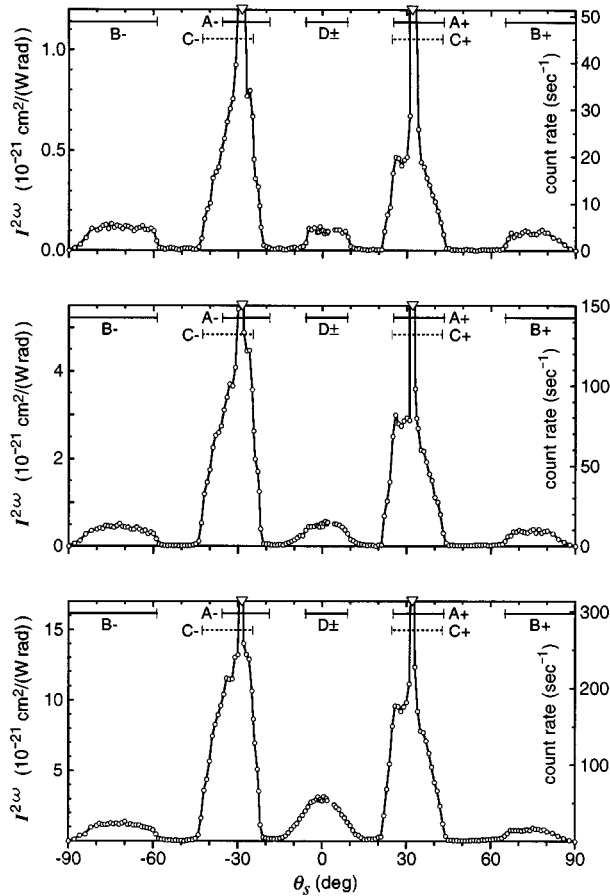


FIG. 6. $I^{2\omega}$ as in Fig. 5, but with expansion of the vertical scale (note varying scales) to show low signal levels. Horizontal lines are coupling ranges discussed in Sec. IV.

$44^\circ < \theta_s < 51^\circ$ with $\theta_i = 8^\circ$. The results of Fig. 8 thus indicate that only these low scattering levels are present with or without the excitation of surface plasmon polaritons at frequency ω . All other far stronger scattering contributions seen for $\theta_i < 15^\circ$ must be intimately connected to surface wave excitation. Indeed, the role of surface plasmon polariton excitation in enhanced second-harmonic generation from a planar silver film was noted some years ago.¹⁴

It is also of interest to consider the area of $I^{2\omega}$. In Figs. 5 and 6 the area is 1.8 , 3.8 , and $9.1 \times 10^{-21} \text{ cm}^2/\text{W}$ for surfaces 1, 2, and 3, respectively. For the case of surface 3 in Figs. 7 and 8, the area is 7.9 , 8.4 , 5.9 , and $0.21 \times 10^{-21} \text{ cm}^2/\text{W}$ for $\theta_i = 0^\circ$, 8° , 13° , and 17° , respectively. These values are somewhat smaller than the specularly reflected second harmonic of approximately $4 \times 10^{-20} \text{ cm}^2/\text{W}$ for oblique incidence angles ($\theta_i \cong 75^\circ$) on a flat silver surface.²

As was expected from the discussion of Sec. II, no back-scattering peak is present in the results of Figs. 5–8. It was also discussed there that we have satisfied conditions required to produce the peak predicted in the direction perpendicular to the mean surface, but surprisingly, this peak is not present in any of our results. In Fig. 9 we show further data taken for surfaces 2 and 3 for small θ_s in a search for this peak; in the case of surface 3 the signals are sufficient to allow the data to be taken with high angular resolution. The peak should be as distinct as the backscattering enhancement of Fig. 3, having an angular width that depends on the fun-

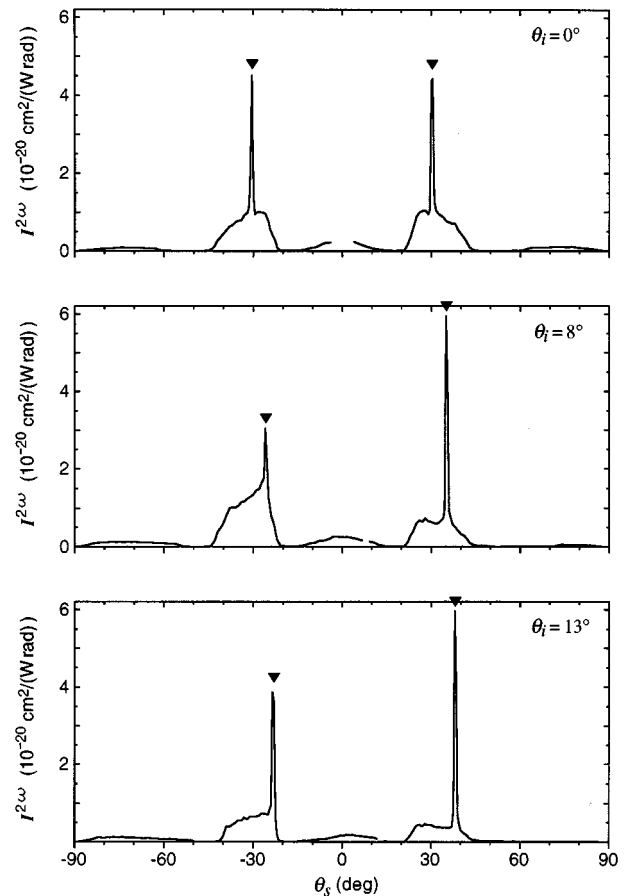


FIG. 7. Diffusely scattered second harmonic $I^{2\omega}$ for surface 3 and the incidence angles θ_i shown. The illumination wavelength is 1064 nm and inverted triangles denote θ_s determined from $k_s(2\omega) = k_i(\omega) \pm k_{sp}(\omega)$. The detector integration angle $\Delta\theta_s = 0.8^\circ$. The break in each curve surrounds the specular reflection.

damental polariton resonance width.³ However, no such peak emerges above the noise levels in any results of Fig. 9.

In view of the high-power levels of these experiments, it is essential to demonstrate here that our data are fully consistent with second-harmonic generation. Many of the tests employed for this purpose are analogous to those used in early studies of second-harmonic generation upon specular reflection from metals.¹ It is shown in Fig. 10 that, for a variety of conditions, the scattered signal at 2ω depends on the square of the incident power, as expected for second-harmonic generation. The following observations were made with surface 3 at $\theta_i = 3^\circ$, but similar tests produced satisfying results for all surfaces. First, it was found that the scattered power (the distribution integrated over all θ_s) fell by 2.0 orders of magnitude upon replacing the 532-nm wavelength detector filter with a similar filter centered at 514 nm. The light at 2ω was well confined to the plane of incidence as expected for one-dimensional roughness; the scattered power decreased by 2.0 orders of magnitude in scanning the detector 1° above or below this plane. This result indicates that the signal could not arise from the more isotropic emission to be expected from thermal effects. The temporal position of the detector time gate was determined by detecting the light at 2ω emitted by a nonlinear crystal placed in the

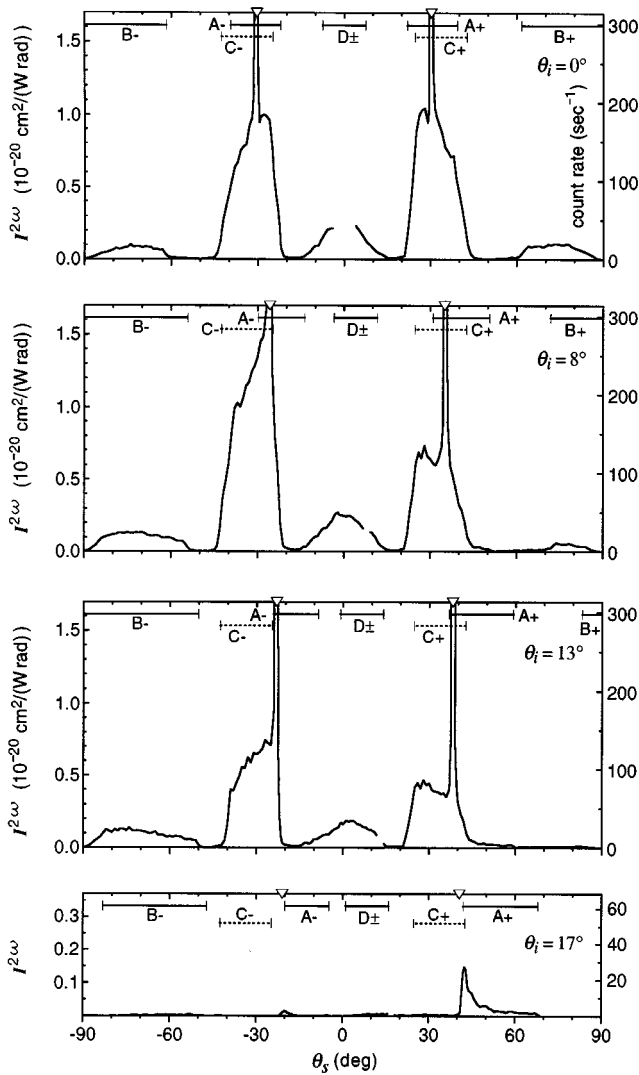


FIG. 8. $I^2\omega$ for surface 3 as in Fig. 7, but with expanded vertical scale. Horizontal lines are coupling ranges discussed in Sec. IV.

sample mount. In the case of surface scatter, monitoring the photocounts arriving in a 5-nsec gate positioned 60 nsec before the arrival of the laser pulse reduced the scattered power by 1.9 orders of magnitude; this provides evidence that the signals were not due to pump or background light. It was

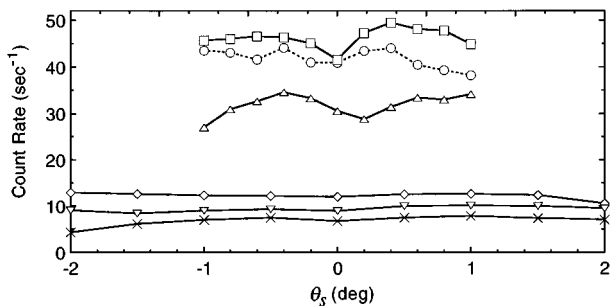


FIG. 9. Diffusely scattered second-harmonic light for surface 2 at $\theta_i=3^\circ$ (diamonds), $\theta_i=9^\circ$ (inverted triangles), and $\theta_i=13^\circ$ (crosses) and for surface 3 at $\theta_i=3^\circ$ (circles), $\theta_i=6^\circ$ (squares), and $\theta_i=13^\circ$ (triangles). The detector integration angle $\Delta\theta_s=0.8^\circ$ (surface 2) and 0.2° (surface 3). No peak appears consistently at $\theta_s=0^\circ$.

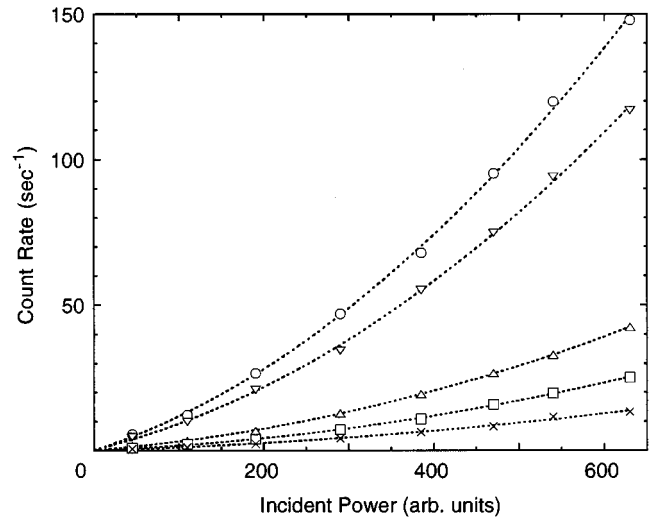


FIG. 10. Dependence of the detected signal at 2ω on the power incident on the sample. For $\theta_i=3^\circ$, the results are for surface 1 at $\theta_s=30^\circ$ (crosses), surface 2 at $\theta_s=29^\circ$ (inverted triangles), and surface 3 at $\theta_s=8^\circ$ (triangles), $\theta_s=29^\circ$ (circles), and $\theta_s=71^\circ$ (squares). Dashed curves are fitted parabolas.

verified that the signals were indeed p polarized as expected; inserting a polarizer to detect s polarization caused the power to fall by 2.7 orders of magnitude. Upon changing the incident wave from p to s polarization, the total (unpolarized) scattered power fell by 1.9 orders of magnitude.

The final component in the incident beam was a filter with transmission 10^{-5} at 2ω and tests were unable to detect signals that could be attributed to light of frequency 2ω incident on the sample. The dark count rate of the photomultiplier was approximately 5000 sec^{-1} , but the contribution to the detected signal is reduced by more than five orders of magnitude by the gating described earlier. The degree to which the detector signal represents isolated 2ω light is suggested by, for example, the remarkably low count rates (0.3 sec^{-1}) seen in the forbidden coupling regions for surface 1 in Fig. 6. Finally, throughout our work there was no visual evidence of surface damage. No differences were seen in linear scattering data taken before and after the nonlinear experiments, nor were changes noted in scans repeated during the course of the second-harmonic measurements.

IV. DISCUSSION

We discuss here a number of aspects of the results presented in Sec. III. We first discuss the lack of a peak normal to the mean surface. Our observations may be unexpected because a number of previous experiments have claimed to observe this peak,^{15,16} but the scattering system that was used is quite different from that of MLA. These experiments have employed Kretschmann prism coupling in a dielectric/semitransparent metal film/nonlinear crystal system,¹⁵ in one case the third medium was free space.¹⁶ Throughout these works the roughness was uncontrolled and uncharacterized and it is not clear which of the two interfaces had the stronger roughness.

In particular, there are some unusual aspects of these results. All peaks observed were 8–12 times higher than background levels,^{15,16} but the mechanism proposed by MLA (the nonlinear interaction of the incident wave and a distribution

having a backscattering peak of at most twice the height of the background¹²) would constrain the peak to a relative height of 2 or less. Also, all linear experiments attempting to observe backscattering enhancement with prism coupling have thus far failed,^{17,18} but this peak must exist in order to make a valid claim to have observed the other peak at 2ω . Further, there is an alternate interpretation of these nonlinear experiments that is unrelated to the mechanisms proposed by MLA. Arnold and Otto¹⁸ have noted that the observed peaks at 2ω could be nothing more than the nonlinear interaction of the prism-coupled plasmon polariton at ω and a similar counterpropagating wave produced by roughness coupling. This nonlinear interaction does not require backscattering enhancement at ω , but has produced light emission at 2ω in a direction perpendicular to a metal surface for counterpropagating plasmon polaritons excited by other means.^{7,19}

It is thus unclear whether previous experiments could have observed the peak at issue. We state our own claims succinctly: we address the simple free-space/metal interface as did MLA; we have demonstrated in Fig. 3 that it produces the necessary linear backscattering peak; $I^{2\omega}$ shows significant levels near $\theta_s = 0^\circ$ in Figs. 5–9, but we do not observe a distinct peak at $\theta_s = 0^\circ$ under any circumstances.

It is also worthwhile to consider the role of lowest-order perturbation theory³ in the results of Sec. III. In particular, this theory predicts that the scatter at 2ω arises from the nonlinear interaction of the incident wave with the lowest-order diffuse scatter of Eq. (3). The wave-vector components parallel to the surface must be conserved, so that the scatter at 2ω is consistent with

$$k_s(2\omega) = k_i(\omega) + [k_i(\omega) \pm k_r] = 2k_i(\omega) \pm k_r. \quad (5)$$

Upon evaluating Eq. (5) for the range of wave number k_r present in Fig. 2, we find that there should be coupling to two relatively narrow angular ranges. These ranges are shown in Fig. 8 [the bars labeled as $A+$ or $A-$ for the sign in Eq. (5)], where scattering consistent with the negative coupling is not clearly seen, but the positive coupling is consistent with the residual scattering levels of $I^{2\omega}$ for $\theta_i = 17^\circ$. As θ_i is reduced, the $A+$ coupling range remains consistent with the motion of these same low levels of $I^{2\omega}$ until they disappear below other scattering contributions for $\theta_i = 0^\circ$. The high peaks are to be considered part of the $A\pm$ coupling for $\theta_i < 15^\circ$ because the scattered waves $k_i(\omega) \pm k_r$ in Eq. (5) include $\pm k_{sp}(\omega)$. The narrow bandwidth of $S(k)$ thus allows direct, unambiguous observations of scatter within angular ranges consistent with lowest-order perturbation theory.

These considerations also make clear that all other components of $I^{2\omega}$ in Figs. 5–8 arise from processes that have not been considered in the context of rough surface scattering. However, we may still identify the origin of these contributions because, first, as discussed in Sec. III, they obviously rely on the excitation of $\pm k_{sp}(\omega)$ and, second, the wave numbers available in $S(k)$ will again restrict the scatter to particular ranges of θ_s . Specifically, we must consider the nonlinear interaction between pairs of fundamental waves with the constraint being, as before, that the parallel wave-vector component must be conserved.

We first consider a nonlinear interaction between the plasmon polariton $\pm k_{sp}(\omega)$ and the single scatter $[k_i(\omega) \pm k_r]$ of Eq. (3), so that the net coupling is $k_s(2\omega) = k_i(\omega) \pm k_{sp}(\omega) \pm k_r$. The scattering ranges consistent with $S(k)$ include evanescent scatter and are labeled as $B\pm$ in Figs. 6 and 8. $I^{2\omega}$ has clear contributions within the $B\pm$ ranges throughout Fig. 6 and, as θ_i increases in Fig. 8, these bands of diffuse scatter move to the right in a manner identical to the predicted coupling. No significant scatter consistent with the $B\pm$ process appears in Fig. 8 at $\theta_i = 17^\circ$ because $\pm k_{sp}(\omega)$ is obviously no longer available to provide the interaction. We thus conclude that we have observed the scattering process $B\pm$ in these experiments.

As was demonstrated in Fig. 4, the harmonic surface wave $\pm k_{sp}(2\omega)$ roughness couples to θ_s within the range ($\pm 25^\circ, \pm 43^\circ$) that is indicated as $C\pm$ in Figs. 6 and 8. It is seen that the diffuse scatter surrounding the high peaks of $I^{2\omega}$ fits well within these coupling regions and that the sloping shape of the distributions is indeed similar to the result of Fig. 4. Further, the angular position of these distributions appears to be independent of θ_i in Fig. 8. This behavior is consistent with the process $C\pm$, which is dependent on $[\pm k_{sp}(2\omega) \mp k_r]$ but independent of $k_i(\omega)$. We thus conclude that $\pm k_{sp}(2\omega)$ remains excited in all cases other than $\theta_i = 17^\circ$ in Fig. 8.

It appears that $\pm k_{sp}(2\omega)$ is excited by the process $B\pm$ described earlier. It is straightforward to calculate that this process indeed produces parallel wave-vector components identical to $\pm k_{sp}(2\omega) = \pm 1.052(2\omega/c)$ throughout the cases discussed with but one interesting exception. For $\theta_i = 13^\circ$, we calculate the minimum parallel wave number produced by the process $B-$ to be $-1.026(2\omega/c)$, which falls short of $-k_{sp}(2\omega)$. Upon comparison with $\theta_i = 8^\circ$, there is only a modest reduction in the height of $I^{2\omega}$ within the $C-$ interval in Fig. 8, which indicates that $-k_{sp}(2\omega)$ is still strongly excited. It has, however, been discussed by Fukui and Stegeman²⁰ that the nonlinear interaction of $\pm k_{sp}(\omega)$ with itself is sufficient to excite $\pm k_{sp}(2\omega)$, even if wave-number matching is not strictly satisfied [i.e., $k_{sp}(2\omega)$ only approximately equals $2k_{sp}(\omega)$]. Thus this mismatched coupling appears to provide the excitation in this particular instance. Further, if this is the case, it is likely that the mismatched coupling would also be significant in all other cases where $\pm k_{sp}(2\omega)$ is excited.

Another possible nonlinear interaction is that of the incident wave with the waves of Eq. (2) that produce the backscattering enhancement in Fig. 3, with the net coupling being $k_s(2\omega) = k_i(\omega) \pm k_{sp}(\omega) \mp k_r$. The scattering ranges consistent with these processes are shown as $D\pm$ in Figs. 6 and 8; the positive and negative ranges overlap. In Fig. 6 a distribution that provides a convincing match with this coupling is seen for surface 1, the fit remains good for surface 2, and a somewhat wider distribution appears for the roughest surface. This nonlinear interaction is indeed the one proposed by MLA having the peak at $\theta_s = 0^\circ$. Hence it is remarkable that the distribution appearing for consistent θ_s is only a featureless rectangular shape spanning the coupling region for surfaces 1 and 2. On the other hand, there is some ambiguity for the relevant linear scattering processes; an identical coupling range is predicted for the interaction of $\pm k_{sp}(\omega)$ with the single scatter $[k_i(\omega) \mp k_r]$ of Eq. (3). In any case, the scatter seen in Fig. 8 for surface 3 exhibits a broader distribution for small θ_s that nevertheless rises within the

$D \pm$ interval, particularly for $\theta_i = 13^\circ$. It is thus possible that the $D \pm$ coupling still appears for surface 3 but is superposed with a broader distribution constrained within $\theta_s = \pm 15^\circ$, but we do not pursue this point further.

We conclude this section by commenting on the minimum perturbation order required to produce the scattering processes observed here. Generally, in the scattered intensity, the perturbation contribution is of the order $(\sigma/\lambda)^{2M}$, where M is the number of roughness couplings required to produce the scattering process of interest. For example, the lowest-order $A \pm$ coupling represents the nonlinear interaction of the unscattered incident wave and the single-scatter of Eq. (3); it thus produces a contribution of order $(\sigma/\lambda)^2$ in the scattered intensity.³ Further, in the $D \pm$ processes the incident wave interacts with a distribution that requires two roughness couplings; a contribution of order $(\sigma/\lambda)^4$ is produced.³ The two interaction waves of the $B \pm$ process each require a single roughness coupling, so that the order here is again $(\sigma/\lambda)^4$. Finally, the $C \pm$ process is produced by the $B \pm$ process, but an additional outward roughness coupling of $\pm k_{sp}(2\omega)$ is necessary; thus the perturbation order is $(\sigma/\lambda)^6$. We note, however, that the σ dependence of the components of $I^{2\omega}$ in Fig. 6 is generally weaker than predicted by these simplistic arguments. This suggests that terms higher than the leading order quoted are already slowing the growth of the scattering contributions with σ .

V. CONCLUSION

Before the experiments described here were conducted, it was not possible to predict what processes would be significant in the production of diffuse second-harmonic light from a rough metal surface. Indeed, it has been seen that lowest-

order perturbation theory is correct in predicting a distribution containing two distinct peaks, but our results are otherwise quite different from those of this theory. Throughout our experiments, we observe that the excitation of plasmon polaritons at frequency ω produces a variety of hitherto unexplained nonlinear interactions. For our relatively narrow rectangular roughness spectrum these interactions are readily identified from their scattering contributions seen within compact angular ranges; such a clear interpretation would probably not be possible for the broad Gaussian spectrum as assumed in theoretical work. Our observed scattering contributions include, for example, clear indications of the nonlinear excitation of surface plasmon polaritons at frequency 2ω . The highly controlled experiments have been essential in drawing such strong conclusions and it is hoped that future theoretical development will benefit from the guidance thus provided.

Despite the theoretical predictions discussed earlier, we have not observed either a backscattering peak or a peak in the direction normal to the surface at 2ω . We did not expect to observe the former peak, but the absence of the latter peak throughout our results was unexpected. We have demonstrated that our surfaces produce the linear couplings required for this peak to exist, and we even observe a distribution at 2ω within a range of scattering angles consistent with the proposed nonlinear process. Nevertheless, the peak of interest is not seen here, and this observation stands as an important issue to be addressed by future theoretical work.

ACKNOWLEDGMENTS

We appreciate the essential help of S. Califano, P. Bartolini, and M. E. Knotts. K.A.O. is grateful for support from the Marchi Foundation.

-
- ¹N. Bloembergen, R. K. Chang, and C. H. Lee, *Phys. Rev. Lett.* **16**, 986 (1966); N. Bloembergen, R. K. Chang, S. S. Jha, and C. H. Lee, *Phys. Rev.* **174**, 813 (1968).
- ²J. E. Sipe and G. I. Stegeman, in *Surface Polaritons*, edited by V. M. Agranovich and D. L. Mills (North-Holland, Amsterdam, 1982).
- ³A. R. McGurn, T. A. Leskova, and V. M. Agranovich, *Phys. Rev. B* **44**, 11 441 (1991).
- ⁴C. K. Chen, A. R. B. de Castro, and Y. R. Shen, *Phys. Rev. Lett.* **46**, 145 (1981).
- ⁵G. S. Agarwal and S. S. Jha, *Phys. Rev. B* **26**, 482 (1982); R. Reinisch and M. Nevière, *ibid.* **28**, 1870 (1983); G. A. Farias and A. A. Maradudin, *ibid.* **30**, 3002 (1984); G. Li and S. R. Seshadri, *ibid.* **44**, 1240 (1991).
- ⁶J. J. Coutaz, M. Nevière, E. Pic, and R. Reinisch, *Phys. Rev. B* **32**, 2227 (1985).
- ⁷G. Blau, J. L. Coutaz, and R. Reinisch, *Opt. Lett.* **18**, 1352 (1993).
- ⁸J. Rudnick and E. A. Stern, *Phys. Rev. B* **4**, 4274 (1971); J. E. Sipe, V. C. Y. So, M. Fukui, and G. I. Stegeman, *ibid.* **21**, 4389 (1980); M. Corvi and W. L. Schaich, *ibid.* **33**, 3688 (1986); D. Maystre, M. Nevière, and R. Reinisch, *Appl. Phys. A* **39**, 115 (1986); J. A. Maytorena, W. L. Mochán, and B. S. Mendoza, *Phys. Rev. B* **51**, 2556 (1995); B. S. Mendoza and W. L. Mochán, *ibid.* **53**, 4999 (1996).
- ⁹D. W. Lynch and W. R. Hunter, in *Handbook of Optical Constants of Solids*, edited by Edward D. Palik (Academic, New York, 1985), p. 356.
- ¹⁰C. S. West and K. A. O'Donnell, *J. Opt. Soc. Am. A* **12**, 390 (1995).
- ¹¹A. R. McGurn, A. A. Maradudin, and V. Celli, *Phys. Rev. B* **31**, 4866 (1985).
- ¹²A. A. Maradudin and E. R. Méndez, *Appl. Opt.* **32**, 3335 (1993).
- ¹³C. S. West and K. A. O'Donnell, *Opt. Lett.* **21**, 1 (1996).
- ¹⁴H. J. Simon, D. E. Mitchell, and J. G. Watson, *Phys. Rev. Lett.* **33**, 1531 (1974).
- ¹⁵X. Wang and H. J. Simon, *Opt. Lett.* **16**, 1475 (1991); Yu Wang and H. J. Simon, *Phys. Rev. B* **47**, 13 695 (1993).
- ¹⁶O. A. Aktsipetrov, V. N. Golovkina, O. I. Kapusta, T. A. Leskova, and N. N. Novikova, *Phys. Lett. A* **170**, 231 (1992).
- ¹⁷A. Steprath, D. Schumacher, A. Otto, and M. Arnold, *Phys. Lett. A* **177**, 433 (1993).
- ¹⁸M. Arnold and A. Otto, *Opt. Commun.* **125**, 122 (1996).
- ¹⁹C. K. Chen, A. R. B. de Castro, and Y. R. Shen, *Opt. Lett.* **4**, 393 (1979).
- ²⁰M. Fukui and G. I. Stegeman, *Solid State Commun.* **26**, 239 (1978).